Solitonlike magnetization textures in noncollinear antiferromagnets

Camilo Ulloa* and A. S. Nunez†

Departamento de Física, Facultad de Ciencias Físicas y Matemáticas, Universidad de Chile, Casilla 487-3, Santiago, Chile

(Received 4 February 2016; revised manuscript received 18 April 2016; published 29 April 2016)

We show that proper control of magnetization textures can be achieved in noncollinear antiferromagnets. This opens the versatile toolbox of domain-wall manipulation in the context of a different family of materials. In this way, we show that noncollinear antiferromagnets are a good prospect for applications in the context of antiferromagnetic spintronics. As in many noncollinear antiferromagnets, the order parameter field takes values in SO(3). By performing a gradient expansion in the energy functional we derive an effective theory that accounts for the physics of the magnetization of long-wavelength excitations. We apply our formalism to static and dynamic textures such as domain walls and localized oscillations, and identify topologically protected textures that are spatially localized. Our results are applicable to the exchange-bias materials Mn_3X, with $X =$ Ir, Rh, Pt.

DOI: 10.1103/PhysRevB.93.134429

I. INTRODUCTION

In antiferromagnetic materials the exchange coupling among neighboring spins favors antiparallel arrangements. Because of this interaction the system is led to an ordered magnetic state where the magnetization of different sublattices is oriented in a way that the overall magnetization is canceled. This order drives the system into a robust collective behavior with soft modes that can be controlled with the aid of external magnetic fields. Recently, the notion that spintronic effects analogous to the ones in ferromagnets can be exhibited by antiferromagnetic systems has received attention from the theoretical [1–5] and experimental [6] viewpoints. The advantages of antiferromagnetic systems come due to a variety of reasons. For example they do not display stray fields, they display high-frequency response (in the terahertz range), and finally the fact that antiferromagnetism is observed more often and at much softer conditions than ferromagnetism.

A promising development in the context of antiferromagnetic spintronics is the fact that it is possible to engineer magnetic textures, such as domain walls (DWs), in antiferromagnetic systems [7]. The problem of domain-wall manipulation in antiferromagnetic systems has been studied in some recent papers [8] where, using the collective coordinates approach, it was shown that the domain-wall center obeys Newton's law of motion. This opens the possibility of implementing domain-wall control over antiferromagnets in the same fashion as it is done in ferromagnets. In ferromagnetic systems magnetization textures, smooth modulations in the magnetization field, can be controlled in a diversity of manners, for example through the action of external fields or currents. Research in the field of magnetic domain-wall manipulation has been growing steadily [9]. The driving force behind this research is the potential applications in the context of information technologies. An example of these applications is the racetrack [10] configuration where domain walls are driven across a ferromagnetic wire by a current. Domain-wall manipulation has also been shown as an alternative to electronic logic circuits [11].

In this paper we propose that magnetic textures can also be found and controlled in noncollinear antiferromagnets—that is, antiferromagnets whose underlying magnetic sublattices are not oriented along the same magnetic axis. Our main result is the theoretical characterization of the dynamics of domain walls in a noncollinear antiferromagnet. While our qualitative results apply to a wide family of noncollinear antiferromagnets, we will focus our attention on the magnetic degrees of freedom Mn_3Ir. This material has been studied extensively due to its importance as the pinning agent in exchange bias controlled spin-valve devices. Mn_3Ir is regarded as a crystal with fcc structure with Mn atoms lying on the centers of the faces of each cube. The Mn sublattices are two-dimensional kagome lattices lying in the planes perpendicular to the (111) direction. Due to the frustration within each triangular plaquette, isolated isotropic kagome lattices are known examples of disordered spin systems [12]. On the contrary the Mn spins in Mn_3Ir display a quite strong three-sublattice triangular ($T1$) magnetic order up to a transition temperature of $\sim$950 K [13]. The stability of magnetic order is due primarily to the exchange interaction among the kagome planes and to anisotropy [14–16]. Following [17], as a minimal model for the physics of the magnetization in Mn_3Ir we start with a single nearest-neighbor antiferromagnetically coupled kagome lattice of classical spins with appropriately tuned anisotropy terms.

II. BASIC MODEL

The minimal model for magnetization dynamics of the Mn atoms in a (111) plane of Mn_3Ir starts from a system of classical spins located at the vertices of a kagome lattice. These spins correspond to the magnetic degrees of freedom of the planes perpendicular to the (111) direction. The Hamiltonian of the spin system contains two main contributions. On one side we have the exchange interaction, characterized by an exchange constant J, between nearest neighbors that favor antiparallel arrangements. On the other we have a strong anisotropy energy that favors orientation in the axis towards the center of the triangles; this energy is characterized by an anisotropy constant K, and an anisotropy that penalizes the out-of-plane orientations characterized by K_z. The resulting Hamiltonian

*camilo.ulloa.o@gmail.com
†alnunez@dfi.uchile.cl

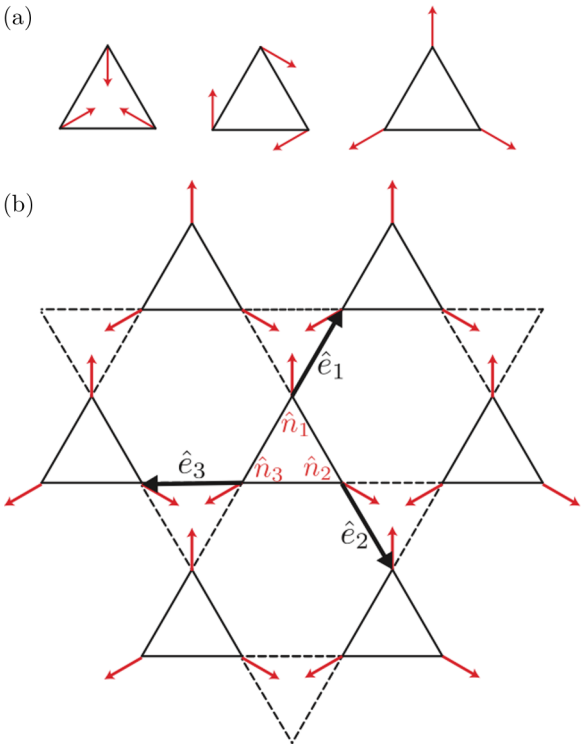

FIG. 1. (a) Different configurations of a given triangle achieved through different rotations around the out-of-plane axes. An arbitrary configuration is encoded by a smooth distribution of such rotations. (b) Kagome lattice in the (111) plane in Mn_3Ir where Mn atoms are at each corner of a basis triangle. The basis vectors $\mathbf{n}_1 = (0,1,0)$, $\mathbf{n}_2 = (\sqrt{3}/2, -1/2, 0)$, and $\mathbf{n}_3 = (-\sqrt{3}/2, -1/2, 0)$ defined at every point in the lattice are shown. The vectors $\mathbf{e}_i$ point towards the nearest neighbors of each site. These vectors are used in the gradient expansion in the continuum approximation and are defined as $\mathbf{e}_1 = (\cos\pi/3, \sin\pi/3, 0)$, $\mathbf{e}_2 = (\cos\pi/3, -\sin\pi/3, 0)$, and $\mathbf{e}_3 = (-1,0,0)$.

becomes

$$\mathcal{H} = J\sum_{\langle \mathbf{r},\mathbf{r}'\rangle} \mathbf{S}_\mathbf{r}\cdot\mathbf{S}_{\mathbf{r}'} - K\sum_{\mathbf{r}}(\mathbf{n}_\mathbf{r}\cdot\mathbf{S}_\mathbf{r})^2 + K_z\sum_{\mathbf{r}}(\hat{\mathbf{z}}\cdot\mathbf{S}_\mathbf{r})^2, \quad (1)$$

where the anisotropy axis, $\mathbf{n}_\mathbf{r}$, is defined on each triangular element of the kagome lattice as illustrated in Fig. 1, and $\hat{\mathbf{z}}$ is the perpendicular axis to the plane. As the antiferromagnetic coupling favors configurations where all the moments in each triangle cancel one another, then if we consider any solid rotation of the moments in one triangle this condition still. Following this idea we start from a given minimum (say, all spins pointing outward) and parametrize the configuration on any point in the lattice by a rotation matrix [18,19]: $\mathbf{S}_\mathbf{r} = \mathcal{R}(\mathbf{r})\{\mathbf{n}_\mathbf{r} + a[\mathbf{L} - (\mathbf{L}\cdot\mathbf{n}_\mathbf{r})\mathbf{n}_\mathbf{r}]\}$, where $\mathbf{L}$ is the canting field assumed to be small. Restricting the description to the low-energy structures we can assume the behavior of the rotation matrix $\mathcal{R}$ to be smooth, varying only across long length scales. Following [18] we write the Lagrangian of the system in terms of the variables $\mathbf{L}$ and $\mathcal{R}$ and express it within the smooth gradient approximation. We then proceed to solve the Euler-Lagrange equations for the field $\mathbf{L}$ finding

$$T\mathbf{L} = \mathcal{R}^{-1}\partial_t\mathcal{R},$$

where $T_{\alpha\beta} = \delta_{\alpha\beta} - \frac{1}{3}\sum_i n_{i\alpha}n_{i\beta}$. Replacing this solution into the action we are led to an effective Lagrangian density involving only the $\mathcal{R}$ field:

$$L = -\frac{\hbar^2}{2\sqrt{3}Ja^2}\mathrm{Tr}[(\mathcal{R}^{-1}\partial_t\mathcal{R})^2] - \mathcal{E}_{\mathrm{ex}}(\mathcal{R}) - \mathcal{E}_{\mathrm{ani}}(\mathcal{R}).$$

The anisotropy coupling favors two configurations: either all spins point toward the center of each triangle or away from it. This state of affairs leaves us with two ground states that are degenerate and the main discussion that follows concerns mainly magnetic textures that connect those states smoothly.

In particular we focus on states that can be obtained from the uniform ground state by a smoothly varying rotation. It is a straightforward calculation to show that a gradient approximation of the exchange energy functional gives us

$$\mathcal{E}_{\mathrm{ex}}[\mathcal{R}] = \frac{Ja^2}{2}\mathrm{tr}(g^{ij}\mathcal{L}_i\,\mathcal{L}_j),$$

where $\mathcal{L}_i = \mathcal{R}^{-1}\partial_i\mathcal{R}$ and $g^{ij}_{\alpha\beta} = e^i_1e^j_1n^3_\alpha n^2_\beta + e^i_2e^j_2n^1_\alpha n^3_\beta + e^i_3e^j_3n^2_\alpha n^1_\beta$. In the last expression the vectors $\mathbf{e}_i$ correspond to the ones defined in Fig. 1(b). The anisotropy contribution to the energy is

$$\mathcal{E}_{\mathrm{ani}}[\mathcal{R}] = -K\sum_i(n^i\cdot\mathcal{R}n^i)^2 + K_z\sum_i(\hat{z}\cdot\mathcal{R}n^i)^2.$$

III. SPIN-WAVE SPECTRA

Now we proceed to analyze the spin wave spectra of the system around the ordered phase [Fig. 2(a)]. Here we call this phase just the homogeneous phase. To achieve this goal we describe the state of the system assuming that $\mathcal{R}$ is a rotation matrix made of Euler angles, $\mathcal{R}(\phi,\theta,\psi) = \mathcal{R}_{Z'}(\psi)\mathcal{R}_X(\theta)\mathcal{R}_Z(\phi)$. Calculating perturbations around the homogeneous phase we derive the effective action for the spin waves. As the perturbations are around the identity matrix, we found that the variables ϕ and ψ correspond to the same rotation. Defining $\chi = \phi + \psi$ the equations of motion are

$$\partial_t^2\chi - \frac{3a^2J^2}{\hbar^2}\nabla^2\chi + \frac{12KJ}{\hbar^2}\chi = 0, \quad (2)$$

$$\partial_t^2\theta + \frac{6J(K+K_z)}{\hbar^2}\theta = 0. \quad (3)$$

The spin-wave spectra is split in a dispersionless flat band with frequency

$$\omega^2 = \frac{6J(K+K_z)}{\hbar^2},$$

independent of the wave vector, and a Klein-Gordon-like branch with frequency

$$\omega^2 = \frac{3a^2J^2}{\hbar^2}k^2 + \frac{12KJ}{\hbar^2},$$

as shown in Fig. 2(b). In the absence of anisotropy the spin-wave branches become $\omega = 0$ and $\omega = vk$ with $v = \sqrt{3}aJ/\hbar$ in agreement with the results of [14,20]. The presence of the flat band is a direct consequence of the absence of interlayer couplings within our model. If we consider interlayer exchange interaction including the terms outside the plane (111) in

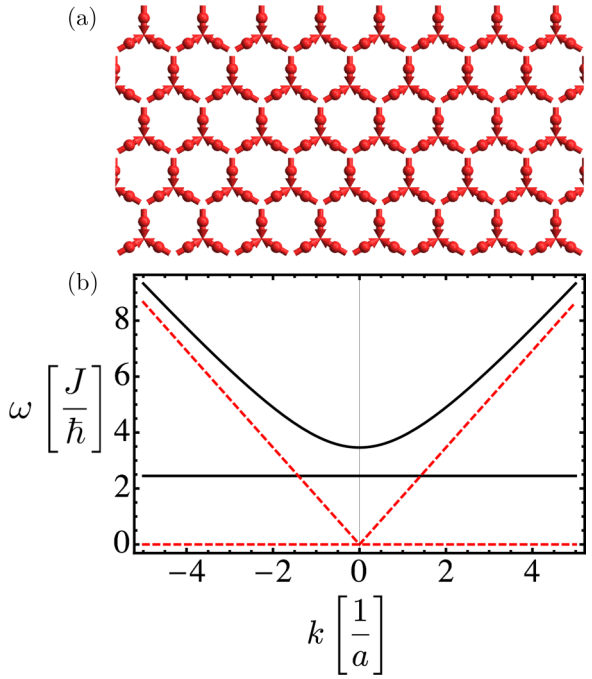

FIG. 2. (a) Homogenous state with all the spins pointing toward the center of the triangles. This state is degenerated with the state with all the spins pointing away from the center of each triangle. (b) Dispersion relations for the spin-wave spectrum of the homogeneous state. Solid lines correspond to the case with anisotropy and describe two branches one being a flat band with zero group velocity and another with a Klein-Gordon-like dispersion. Dashed line represents the dispersion relations of the isotropic case.

the gradient expansion, the flat band is modified as shown in [14,21].

IV. SOLITONLIKE STRUCTURES

We continue our discussion on magnetic textures looking at possible DWs in the order-parameter field. We parametrize the rotation at each point by an angle ϕ and a rotation axis parallel to the z axis (out of the plane). The Lagrangian density can be expressed in terms of ϕ:

$$L = \frac{\hbar^2}{\sqrt{3}Ja^2}(\partial_t\phi)^2 - \sqrt{3}J(\nabla\phi)^2 + \frac{4\sqrt{3}K}{a^2}\cos^2\phi.$$

This corresponds to the well-known sine-Gordon model whose equation of motion is

$$\partial_t^2\phi - c^2\nabla^2\phi + \frac{m^2c^4}{\hbar^2}\sin(2\phi) = 0,$$

where we have defined the spin-wave velocity $c^2 = 3J^2a^2/\hbar^2$ and the mass parameter $m^2c^4/\hbar^2 = 6KJ/\hbar^2$. The solutions of this equation have been extensively studied [22]. Among its most celebrated solutions we can highlight stationary domain walls (where the angle travels all the way from zero to π) that are characterized by a domain-wall width $W = a\sqrt{J/K}/2$. For Mn_3Ir rough estimates of the parameters lead us to $W \sim 1$–$10a$ [15]. The profile of the domain wall has a solitonlike form: $\phi = 2\tan^{-1}[\exp(x/W)]$ [Fig. 3(b)]. To characterize the

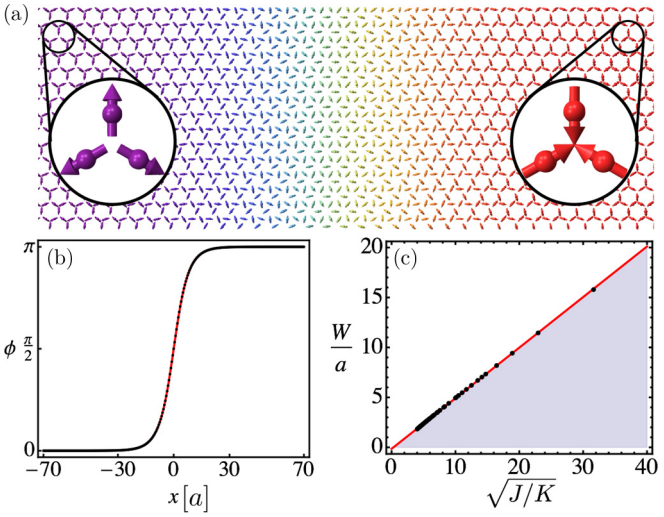

FIG. 3. (a) Typical shape of a domain wall in kagome lattice. (b) Numerical fit of the soliton solution, black dots are the result of numerical simulation, red line corresponds to fitted solution $\phi = 2\tan^{-1}[\exp(x/W)]$. (c) Width dependence on anisotropy. Black dots are numerical results while red dashed line is the fitted curve which has a slope equal to 1/2.

domain walls we have solved numerically the Landau-Lifshitz-Gilbert equation with an effective field derived from Eq. (1). By setting periodic boundary conditions in the exchange field we have enforced a domain wall within our system and let the system relax. The domain-wall profile is then optimized and its width determined by fitting to a solitonlike shape with adjustable width. The results are displayed in Fig. 3 and are in remarkable agreement with the long-wavelength description of the continuum model.

Along with the stationary domain walls just described the sine-Gordon model allows for mobile textures. As is well known, the profile of a domain wall moving with velocity v is contracted by the Lorentz factor leading to a solution $\phi = 2\tan^{-1}\{\exp[(x - vt)/W_0\sqrt{1-(v/c)^2}]\}$. We have verified this behavior using our simulations based on the Landau-Lifshitz equation. The results are shown in Fig. 4(a).

Among the other localized excitations that are associated with the sine-Gordon equation, we have focused on the stationary breather solution [23], $\phi = 2\tan^{-1}[\sqrt{1-\omega^2}\cos(\omega t/\tau)/\omega\cosh(x\sqrt{1-\omega^2}/\lambda)]$, where $\tau = \hbar/mc^2\sqrt{2}$, and $\lambda = \hbar/mc\sqrt{2}$. This solution represents a localized oscillation of the orientation of the local moments around the anisotropy axes. The numerical solution of the Landau-Lifshitz equation that is consistent with this state is shown in Figs. 4(b) and 4(c).

V. TOPOLOGICAL DEFECTS

The topology of the order parameter space [SO(3)] opens a variety of possible topologically protected defects [24]. For example, the first homotopy group being $\pi_1[\mathrm{SO}(3)] = \mathbb{Z}_2$, we have two kinds of configurations. While textures which belong to class 0 can be continuously deformed to the uniform state, textures which belong to class 1 cannot. The latter are known as disgyrations in the context of ^{3}He. The coalescence

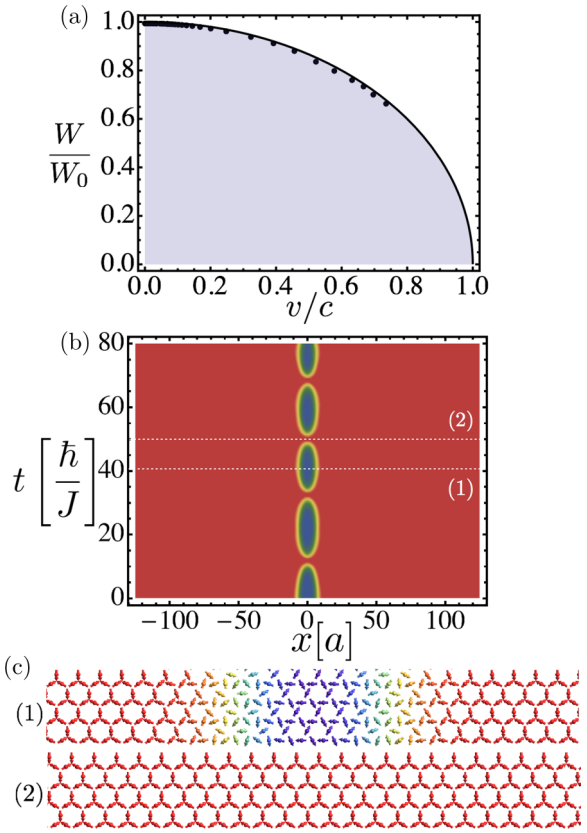

FIG. 4. (a) Contraction of the width W of a moving DW as function of speed v. The simulations were performed setting the easy axis anisotropy by $K = 0.025J$, and the hard axis anisotropy by $K_z = 0.1J$. The results of the Landau-Lifshitz equation shows perfect agreement with the Lorentz contraction factor $\sqrt{1-(v/c)^2}$, full line, that can be inferred from the sine-Gordon equation. (b) Time evolution of the orientation ϕ in the case of a breather state with frequency $\omega = 0.25$. The results correspond to the solution of the Landau-Lifshitz equation with the same parameters as in Fig. 4(a). The color code is the same as the one used for the DW. (c) Snapshot at time (1) and (2) showing the orientation of the local moments in the texture.

of two disgyrations generates a vortexlike trivial texture (as a consequence of $1 + 1 = 0$). However, disgyrations have an energy that grows with system size then are not localized.

The second homotopy group of $\pi_2[\mathrm{SO}(3)]$ is trivial and skyrmions are not topologically protected. Nevertheless there are trivial stable solutions such as the *lump* solution [23]. In Fig. 5 we show examples of textures related with the previous topological properties.

Finally, the third homotopy group of the order-parameter space is given by $\pi_3[\mathrm{SO}(3)] = \mathbb{Z}$ which opens up the possibility of topologically stable pointlike defects. Physical realizations of this kind of topological defects have been studied in the context of superfluid ^{3}He-A [25] and topological insulators [26]. Our description of a single kagome lattice needs to be extended to include interplane interactions in the gradient expansion. In this case the topological defect is a three-dimensional structure characterized by covering all possible rotations as we move away from its center. The winding number associated with the third homotopy group

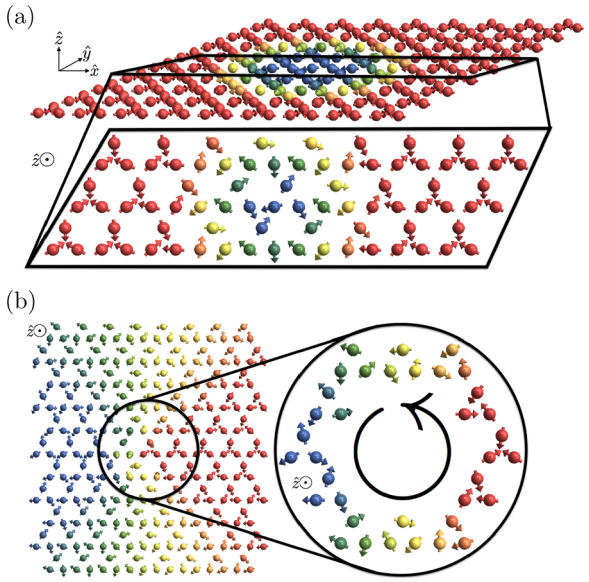

FIG. 5. (a) Cartoon of a *lump* texture, given by the parametrization $\mathcal{R}(\eta,\hat{z})\mathbf{n}_\mathbf{r}$, where $\eta(r) = 2\arctan[\exp(r-R)/W]$. This is an example of a trivial two-dimensional texture. While this solution is stable, it has no topological protection at all so it can be continuously deformed to the homogeneous state. (b) Cartoon of a class 1 disgyration. This solution is topologically protected because of the nontrivial homotopy $\pi_1[\mathrm{SO}(3)]$, then it is not possible to reach the homogeneous state adiabatically. As this state is not localized, its energy grows with the size of the system.

is given by [27–29]

$$Q = \frac{1}{24\pi^2}\int dr\ \varepsilon_{\mu\nu\lambda}\mathrm{tr}(\mathcal{L}_\mu\mathcal{L}_\nu\mathcal{L}_\lambda),$$

where ε stands for the fully antisymmetric tensor. One possible realization of this kind of defect is the Shankar monopole [30]. The idea is to associate to each point of space $\vec{r} = r\hat{n}$ an operator that rotates around the $\hat{n}$ axis an angle $\chi(r)$. If χ is chosen to go all the way from zero at the origin to 2π away from the monopole we can see that the whole parameter space is covered twice. The texture so generated is stable under perturbations and becomes a finite-energy topologically protected defect.

VI. CONCLUSIONS

In this paper we have addressed the behavior of textures in the order-parameter field of noncollinear antiferromagnets. By pursuing a continuum description of the textures we have studied the spin-wave spectra around the homogeneous configuration and the behavior of domain walls. The spin-wave spectra consist of two branches. One corresponds to the usual Klein-Gordon-like dispersion relation while the other corresponds to a flat band whose frequency is independent of the wave number. Domain-wall structure behaves in a similar fashion to Bloch-type domain walls in common ferromagnets with a characteristic with scaling with the square root of J/K (exchange interaction compared with anisotropy). They are described by an effective sine-Gordon equation that allows us to predict the existence, along with stationary domain walls, of

moving domain walls that travel undistorted across the system. We have compared the predictions of our continuum theory with the results of exact simulations of the Landau-Lifshitz-Gilbert equation and obtained a complete agreement.

Finally we have discussed the topological defects that are allowed by the topology of the order parameter space.

ACKNOWLEDGMENT

The authors acknowledge funding from Proyecto Fondecyt Grant No. 1150072, Proyecto Basal Grant No. FB0807-CEDENNA, and Anillo de Ciencia y Tecnonología Grant No. ACT 1117

[1] A. H. MacDonald and M. Tsoi, Philos. Trans. R. Soc. London A **369**, 3098 (2011); R. Duine, Nat. Mater. **10**, 344 (2011).

[2] A. S. Nunez, R. A. Duine, P. Haney, and A. H. MacDonald, Phys. Rev. B **73**, 214426 (2006); P. M. Haney, D. Waldron, R. A. Duine, A. S. Nunez, H. Guo, and A. H. MacDonald, *ibid.* **75**, 174428 (2007).

[3] E. V. Gomonay and V. M. Loktev, Low Temp. Phys. **40**, 17 (2014).

[4] A. S. Nunez, Solid State Commun. **198**, 18 (2014).

[5] R. E Troncoso, C. Ulloa, F. Pesce, and A. S. Nunez, Phys. Rev. B **92**, 224424 (2015).

[6] S. Urazhdin and N. Anthony, Phys. Rev. Lett. **99**, 046602 (2007); Z. Wei, A. Sharma, A. S. Nunez, P. M. Haney, R. A. Duine, J. Bass, A. H. MacDonald, and M. Tsoi, *ibid.* **98**, 116603 (2007); P. M. Haney and A. H. MacDonald, *ibid.* **100**, 196801 (2008); Y. Xu, S. Wang, and K. Xia, *ibid.* **100**, 226602 (2008); H. V. Gomonay and V. M. Loktev, Phys. Rev. B **81**, 144427 (2010); H. V. Gomonay, R. V. Kunitsyn, and V. M. Loktev, *ibid.* **85**, 134446 (2012).

[7] J. M. Logan, H. C. Kim, D. Rosenmann, Z. Cai, R. Divan, O. G. Shpyrko, and E. D. Isaacs, Appl. Phys. Lett. **100**, 192405 (2012).

[8] B. A. Ivanov and A. K. Kolezhuk, Fiz. Nizk. Temp. **21**, 355 (1995) [Low Temp. Phys. **21**, 275 (1995)]; K. M. D. Hals, Y. Tserkovnyak, and A. Brataas, Phys. Rev. Lett. **106**, 107206 (2011); A. C. Swaving and R. A. Duine, Phys. Rev. B **83**, 054428 (2011); R. Cheng and Q. Niu, *ibid.* **86**, 245118 (2012); E. G. Tveten, A. Qaiumzadeh, O. A. Tretiakov, and A. Brataas, Phys. Rev. Lett. **110**, 127208 (2013); E. G. Tveten, T. Müller, J. Linder, and A. Brataas, Phys. Rev. B **93**, 104408 (2016).

[9] J. Shibata, G. Tatara, and H. Kohno, J. Phys. D: Appl. Phys. **44**, 384004 (2011).

[10] S. S. P. Parkin, M. Hayashi, and L. Thomas, Science **320**, 190 (2008).

[11] K. A. Omari and T. J. Hayward, Phys. Rev. Appl. **2**, 044001 (2014).

[12] A. Chubukov, Phys. Rev. Lett. **69**, 832 (1992); D. A. Huse and A. D. Rutenberg, Phys. Rev. B **45**, 7536 (1992); S. Sachdev, *ibid.* **45**, 12377 (1992); I. Ritchey, P. Chandra, and P. Coleman, *ibid.* **47**, 15342 (1993).

[13] A. Kohn, A. Kovacs, R. Fan, G. J. McIntyre, R. C. C. Ward, and J. P. Goff, Sci. Rep. **3**, 2412 (2013); I. Tomeno, H. N. Fuke, H. Iwasaki, M. Sahashi, and Y. Tsunoda, J. Appl. Phys. **86**, 3853 (1999).

[14] M. D. LeBlanc, M. L. Plumer, J. P. Whitehead, and B. W. Southern, Phys. Rev. B **88**, 094406 (2013).

[15] L. Szunyogh, B. Lazarovits, L. Udvardi, J. Jackson, and U. Nowak, Phys. Rev. B **79**, 020403(R) (2009).

[16] V. Hemmati, M. L. Plumer, J. P. Whitehead, and B. W Southern, Phys. Rev. B **86**, 104419 (2012).

[17] H. Chen, Q. Niu, and A. H. MacDonald, Phys. Rev. Lett. **112**, 017205 (2014).

[18] T. Dombre and N. Read, Phys. Rev. B **39**, 6797 (1989).

[19] A. F. Andreev and V. I. Marchenko, Phys. Usp. **23**, 21 (1980).

[20] A. B Harris, C. Kallin, and A. J Berlinsky, Phys. Rev. B **45**, 2899 (1992).

[21] E. V. Gomonaj and V. A. Lvov, J. Magn. Magn. Mater. **86**, 301 (1990); Phase Trans. **38**, 15 (1992).

[22] R. Rajaraman, *Solitons and Instantons: An Introduction to Solitons and Instantons in Quantum Field Theory* (Elsevier, Amsterdam, 1987).

[23] J. Cuevas-Maraver, P. G Kevrekidis, and F. Williams, *The Sine-Gordon Model and its Applications* (Springer International, Switzerland, 2014).

[24] N. D. Mermin, Rev. Mod. Phys. **51**, 591 (1979).

[25] M. Nakahara, *Geometry, Topology and Physics* (IOP, Bristol, 2003).

[26] Y. Zhang, Y. Ran, and A. Vishwanath, Phys. Rev. B **79**, 245331 (2009).

[27] R. Jackiw, in *Current Algebra and Anomalies*, edited by S. B. Treiman *et al.* (Princeton University Press, Princeton, 1985).

[28] A. M. Polyakov, *Gauge Fields and Strings* (Harwood, Chur, 1987).

[29] O. Gomonay, Phys. Rev. B **91**, 144421 (2015).

[30] R. Shankar, Phys. Rev. D **14**, 1107 (1976).